JOURNAL OF THERMOPHYSICS AND HEAT TRANSFER
Vol. 14, No. 2, April–June 2000

New Inductively Heated Plasma Source for Reentry Simulations

G. Herdrich,* M. Auweter-Kurtz,† and H. Kurtz‡
University of Stuttgart, D-70550 Stuttgart, Germany

Magnetoplasmadynamicplasma generators (MPG), thermal arcjet devices and inductively heated plasma generators (IPG) have been developed for thermal protection system material tests at the Institut für Raumfahrtsysteme. Because of the design of the IPG, no electrode erosion appears; plasma impurities are minimized. Hence, the behavior of gas components can be examined individually and basic material tests (e.g., catalytic behavior) can be performed. The IPG3's induction coil is closer to the plasma than it was with previous designs, leading to a reduction of electromagnetic losses. The water cooling system surrounds the coil and the tube. IPG3 was qualified up to an anode power of 180 kW (argon), which is an improvement regarding the planned reentry simulations in combination with the MPG plasma wind tunnels (PWK). The structures of IPG3 and the facility PWK3 are presented. First experimental results such as power characteristics are given. Frequency measurements were made, which will be a help for later numerical simulations of IPG3. A charge injection device camera was used to measure the radial intensity of the IPG3 plasma. The results led to a rough determination of the skin depth.

Nomenclature

A	= related to resonant circuit anode
a	= fit function constant
b	= fit function constant
c	= fit function constant
f	= frequency, Hz
I_A	= anode current, A
ng	= related to plasma-off mode
operate	= related to plasma-on mode
P_A	= anode power, W
plasma	= related to plasma
U_A	= anode voltage, V
δ	= skin depth, m
η	= efficiency
μ_0	= permeability, $(V \cdot s)/(A \cdot m)$
σ	= electrical conductivity, Ωm
ω	= angular frequency, 1/s

Introduction

FIVE plasma wind tunnels (PWK 1–5) are in operation at the Institut für Raumfahrtsysteme (IRS) to reproduce the thermal, aerodynamic, and chemical load on the surface of a space vehicle entering a celestial body's atmosphere. Two of these PWK are equipped with magnetoplasmadynamic plasma generators (MPG), which allow gas flows to be produced on high enthalpy levels. They are mainly used to investigate the erosion of radiation-cooled heat shield materials like C–C or C–SiC, as well as the behavior of ablative materials under thermal and chemical loads. Furthermore, a thermal arcjet device producing moderate enthalpies and higher stagnation pressures to simulate the follow-on flight path is in operation.[1] In comparison with the MPG generators and the arcjet devices, two main advantages are evident when using the inductively heated plasma generators (IPG). One basic aim of reentry material experiments is the investigation of the catalytic behavior. Because of the electrode erosions of the MPG generator as well as of the arcjet device, plasma pollution is present that leads to unwanted chemical reactions in front of the material probe. As the IPG has no electrodes, no electrode erosion is expected. Therefore, the behavior of the probe and the plasma in front of it can be considered to be unadulterated. This means that the catalytic behavior of the material probes can be investigated, and a comparison between the inductively heated plasma and the arc-heated plasma can be made. The second advantage also results from the inductively coupled power input: Even rather reactive gases (O_2, CO_2) can be applied. Hence, atmospheres of celestial bodies like Mars or Venus can be simulated. The influence of the single gas components can be investigated, for example, with regard to the catalytic behavior of a material.

Inductively heated PWK have been qualified due to their decisive advantages allowing basic thermal protection systems (TPS) material investigations and the reentry simulation of celestial bodies like Mars or Venus. Investigations of the catalytic behavior of TPS-related materials have already been performed at the Institute for Problems in Mechanics, Russian Academy of Science. Here a set of inductively heated plasma generators was used to investigate materials in subsonic dissociated carbon dioxide plasma flows.[2,3]

Furthermore, a plasmatron facility operating at anode powers up to 1.2 MW is being qualified at the Von Kármán Institute in Belgium. Here a mapping of the plasmatron's operational envelope has been made.[4]

Powerful measurement techniques like intrusive probes and nonintrusive methods like emission spectroscopy, laser-induced fluorescence (LIF) and Fabry–Perot interferometry (FPI) are used at the IRS to investigate the plasma flows.[5]

To measure the plasma power of the IRS–IPG3, the resonant circuit was run in a no-plasma mode. In a second step the resonant circuit was run in plasma mode having the tube conditions kept constant. The corresponding power values lead to a good estimation of the plasma power.[6] With this a tool to adjust the desired plasma conditions is provided.

The plasma generator IPG3 is made up five main parts. The injection head enables different gas injection angles because the inner gas injection head can be replaced with others with different bore angles. The tube contains the produced plasma, which leaves the generator through the water-cooled chamber adapter. The induction coil is connected to the external resonant circuit, which delivers power and high-pressure cooling water. The magnetic field provided by the induction coil induces circumferential currents in the plasma. These currents depend on the frequency of the resonant circuit and the electrical conductivity of the plasma. Furthermore, both the tube and the coil are surrounded by the external tube cooling, which protects the tube from overheating.

Received 6 July 1999; revision received 28 October 1999; accepted for publication 28 October 1999. Copyright © 2000 by the authors. Published by the American Institute of Aeronautics and Astronautics, Inc., with permission.

*Research Engineer, Institut für Raumfahrtsysteme, Pfaffenwaldring 31.
†Professor, Institut für Raumfahrtsysteme, Pfaffenwaldring 31. Senior Member AIAA.
‡Head of Laboratory, Institut für Raumfahrtsysteme, Pfaffenwaldring 31.

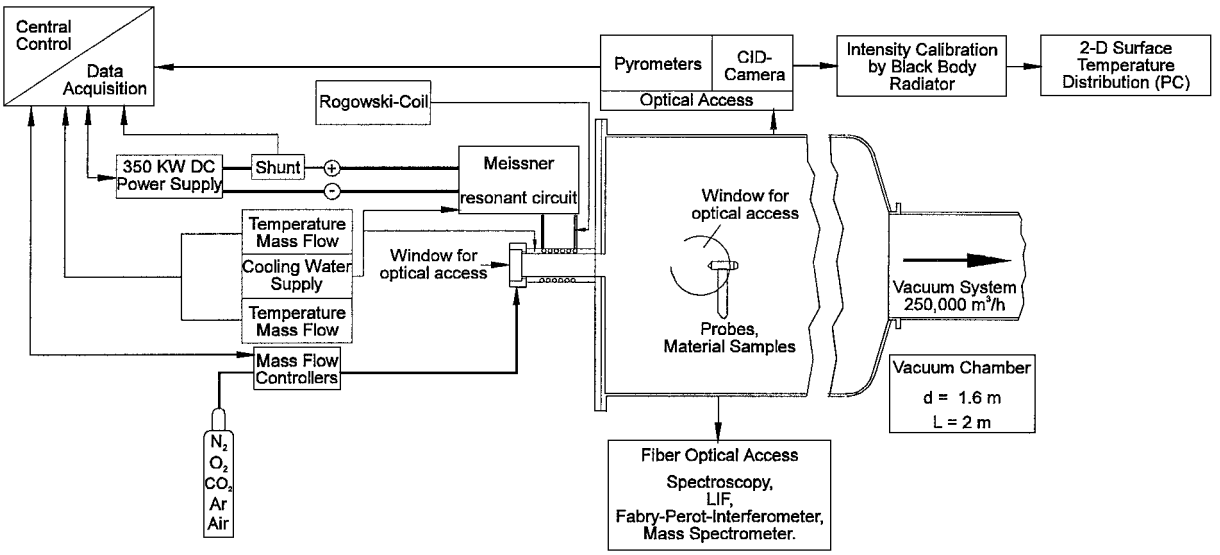

Fig. 1 Schematic of PWK3 and IPG3.

Setup of PWK3 and IPG3

PWK3

The basic setup of the PWK3 together with IPG3 is shown in Fig. 1. The whole experimental setup consists of the plasma source IPG3 and the vacuum chamber. The size of the vacuum chamber is about 2 m in length and 1.6 m in diameter. Optical accesses to the vacuum chamber are provided to measure and observe the plasma. A heat exchanger is used between the test chamber and the vacuum system to cool down the hot plasma. The plain lid of PWK3 (left side of chamber; Fig. 1) carries the IPG3 and the external resonant circuit, which consists of the capacitors with the connection to the plasma generator. The right-side flange of the vacuum chamber is connected to the IRS roots pump system.

Resonant Circuit

The external resonant circuit is cooled by a water cooling circuit. With this, the capacitors, which have a capacity of 6000 pF ± 20% each, and the induction coil are cooled. The resonant circuit is built in Meissner-type switching[7] using a metal–ceramic triode with an oscillator efficiency of about 75%.[8] Its nominal frequency can be changed by switching the different orders or amounts of capacitors (Fig. 2) as well as by the use of coils with different inductivities. The error bars in Fig. 2 take into account the tolerances of the capacitors.

For the present investigations it is tuned to a nominal frequency of 0.54 MHz using a water-cooled, five-turn coil with a length of about 120 mm. The whole circuit is switched to a 375-kW power supply. The incoming anode power can be adjusted by the control of the anode voltage.

IPG3

The principal parts of the plasma generator IPG3 are described here. Various gas injection angles are achievable by replacing the inner gas injection head with others that have different bore angles (Fig. 3). Therefore, the influence of the injection angle to the operational behavior of IPG3 can be studied. It is evident that the plasma is continuously swept away by an axially injected gas.[9] Therefore, the plasma can be stabilized using a tangential injection of the gas.

In addition, lower pressure can be expected in the tube's center. Thus, on the one hand the plasma partially recirculates, on the other hand it is partially kept away from the inner surface of the tube. Hence, a lower heat load of the tube can be achieved and higher power can be applied. An axial optical access through the inner injection head enables investigations of the plasma inside the generator. Figure 3 schematically shows the optical access, and Fig. 4

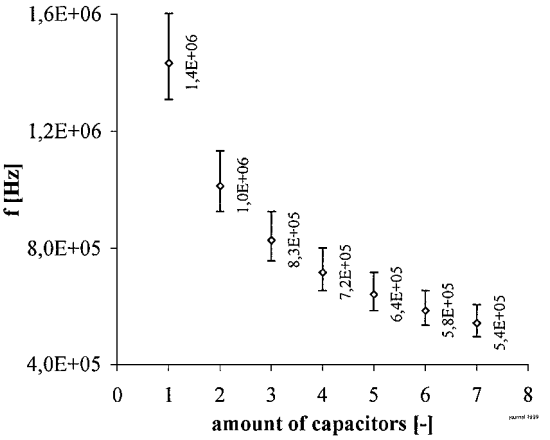

Fig. 2 Nominal operating frequencies for different capacitor switchings.

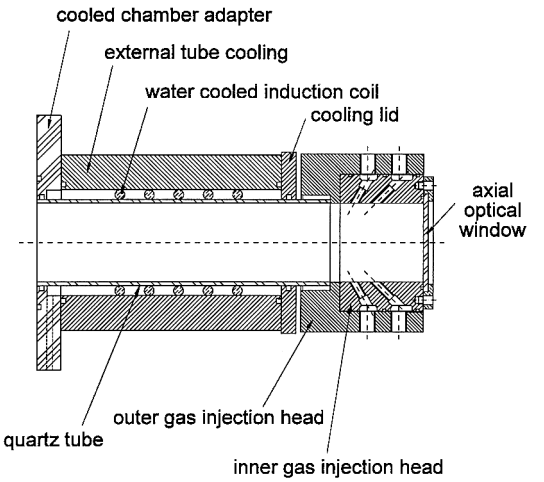

Fig. 3 View of plasma source IPG3.

shows the optical window of IPG3 while it is in operation with argon. The tube cooling system is transparent; therefore, the position of the plasma flame within the tube can be observed with regard to different operating parameters such as chamber pressure, gas, mass flow, and anode power. Additionally, this feature is supported by the axial optical window.

The quartz tube contains the produced plasma that leaves the generator through the water-cooled chamber adapter. The induction

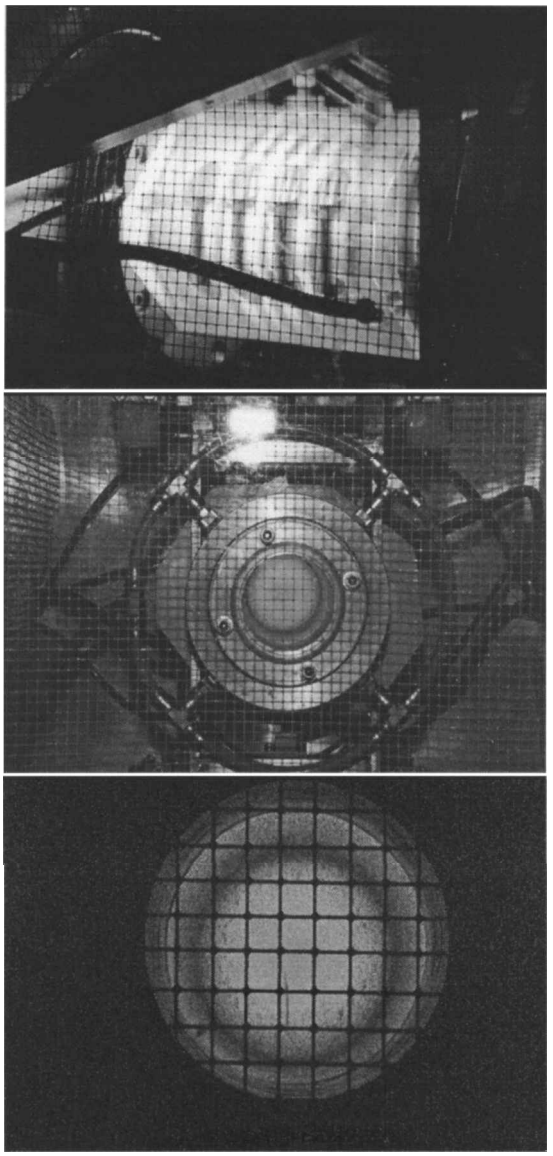

Fig. 4 Plasmagenerator IPG3 in operation (argon): top, side view, and middle and bottom, axial optical window.

coil is connected to the external resonant circuit (Fig. 1) that delivers power and cooling water for IPG3. The magnetic field provided by the induction coil induces circumferential currents in the plasma. These currents depend on the frequency of the resonant circuit and the electrical conductivity of the plasma. Furthermore, both the tube and the coil are surrounded by the external tube cooling, which protects the quartz tube from overheating. The water and an additional cage around the generator serve as an rf-radiation protection shield. Figure 4 shows IPG3 and its tube cooling while operating with argon. The top picture in Fig. 4 shows a side view of IPG3, and the middle and lower pictures show the axial optical access of IPG3. The total length of IPG3 is about 0.35 m, and its diameter is about 0.1 m.

Measurement Techniques

Diagnostics

A variety of probes such as material probes and mechanical probes to measure dynamic pressure, enthalpy, and heat load were developed and can be installed in PWK3. Electron temperature measurements with electrostatic probes are envisaged. Such investigations have already been performed in the IRS-facilities PWK1 and 2.[10] It is evident that the qualification of an electrostatic probe measurement system using an IPG is quite a challenging task due to the field oscillations. However, such measurements have already been performed successfully by van Ootegem et al. with argon as working gas using the CORIA IPG-facility.[11] Rear side temperatures of material samples can be measured with a miniaturized linear pyrometer.[12] All probes can be positioned in the chamber using an electrical positioning system. Hence, with the adjustment of generator power, vacuum chamber pressure, probe positions, and mass flow of the plasmagenous gas, reproduceable simulation points are possible.

Optical diagnostic measurement techniques such as emission spectroscopy for the determination of rotational and vibrational temperatures, FPI to measure plasma velocities and translational temperatures, and LIF for the measurement of atomic species densities are used to characterize the plasma. Different spectral pyrometers are applied to measure the front side temperatures of the investigated material samples.[5] To determine the emissivities a measurement facility based on blackbody radiation is qualified.

Apart from the aforementioned intrusive probes, a quadrupole mass spectrometer to investigate the catalytic behavior of the reentry materials[13,14] is available. The complete mass spectrometer will be placed inside PWK3 fixed on the coordinate table.

IPG3 Measurement Equipment

The Meissner-type resonant circuit is supplied by the dc anode power P_A that is measured during the operation of the device.[7] The anode voltage U_A is controlled. Hence, the anode current I_A results from the load of the resonant circuit (plasma) and the accompanying operating conditions.

Thermal powers such as tube cooling power, resonant circuit power, and plasma power are measured using resistance thermometers (see Fig. 1). They are electrically sealed and, additionally, installed at an acceptable distance from the plasma source to hinder disturbing signals from the rf field. Furthermore, the cooling water flow rates are measured.

A calorimeter for the measurement of the plasma power in the PWK3 is presently undergoing qualification. In addition, the mass flow of the gas is measured and the pressure of the inner gas injection head is measured. A Rogowski coil is used to determine the operational frequencies.

Measurements

Frequencies

The frequency was measured using a coil that was wrapped around one of the inductor connections (see Fig. 1). All measurements were performed at a vacuum chamber pressure of about 100 Pa at a mass flow rate of 1.5 g/s with air as well as with argon. The gases were tangentially injected. The measurements were made using air and argon with different anode powers. Figure 5 shows the determined frequencies for argon and air vs the anode power P_A. The mean value for the frequency in air operation is 510 kHz; the mean value for argon is 528 kHz. The different frequencies can be most likely explained by the different field dampings due to the mutual inductions, which lead to a change of the inductivity. This again changes the operational frequency.

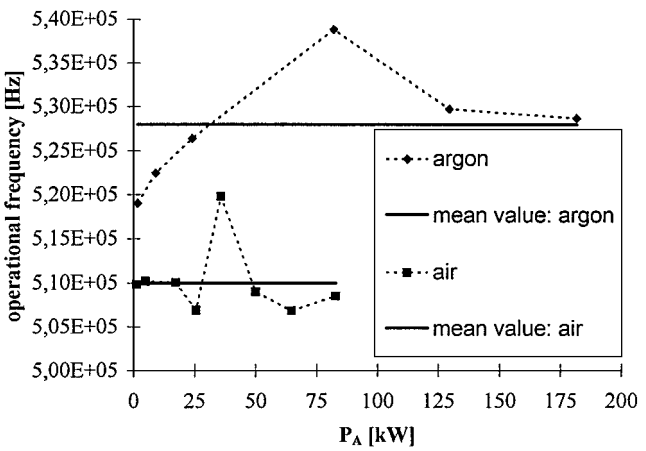

Fig. 5 Operational frequencies (argon and air).

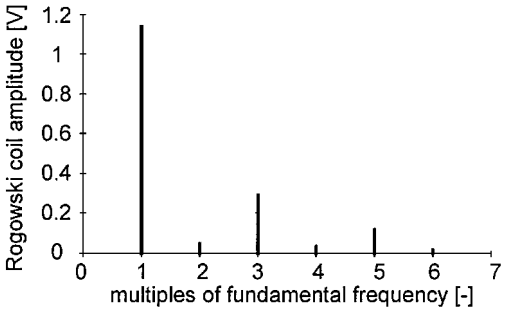

Fig. 6 Amplitudes of the fundamental frequency and overtones for air operation.

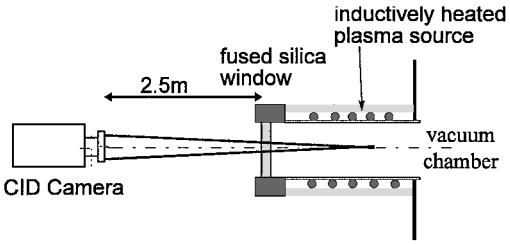

Fig. 7 CID camera measurements.

The data were measured with a Kontron transient recorder. Figure 6 shows an example for a Fourier-analyzed data array measured while the IPG3 was operated with air at 1.5 g/s and a pressure of about 100 Pa. It can be seen that the fundamental frequency 510 kHz dominates. All further amplitudes decrease with increasing multiple of the fundamental frequency.

Radial Intensity Distribution

A charge injection device (CID) camera was used to investigate the transition between low-power mode discharge and high-power mode discharge and the radial intensity distribution for air operation. Figure 7 shows the optical measurements.

The spectral response of the CID camera ranges between 0.1 and 0.15 A/W in the wavelength interval between 400 and 800 nm. However, wavelengths lower than 400 nm and greater than 800 nm still contribute a signal due to the lower spectral responses. The measurement was done through the axial optical window of IPG3. This window is a fused silica glass that delivers transmissions of about constant 0.92 in the wavelength range between 270 and 900 nm. The focus of the camera was about 5 cm behind the closest coil winding, the camera's distance to the axial outlet was about 2.5 m. Therefore, the rf-protection cage meshes could be used as a geometric net enabling the introduction of the tube's diameter geometry (Fig. 8).

The camera has a spectral response in a wide wavelength range leading to an arbitrary intensity distribution; therefore, the data were normalized subject to the measured maximum. The ambient pressure in the vacuum chamber was about 100 Pa. Both argon and air were injected tangentially with a mass flow of 1.5 g/s. The discharge transition for argon is rather faded on the one hand; on the other hand, the required resonant circuit's anode input power P_A is about 5 kW and is much lower than in the case with air.

The discharge transition for air appeared at a power level of $P_A \approx 17$ kW, where the anode voltage was switched from $U_A \approx 3300$ to 4000 V. Between these two values the operational state was unstable. The intensities seemed to jump back and forth between the two operational states. The transition can probably be explained by the magnetic blocking. This blocking is represented by a field coming from the plasma current that counteracts the field of the coil (Lenz's law). While in the low-power mode, the electrical conductivity of the plasma and, hence, the blocking are low, which may lead to the maximum in the middle of the tube; the blocking increases with increasing power leading to the mode change (Fig. 9). From there

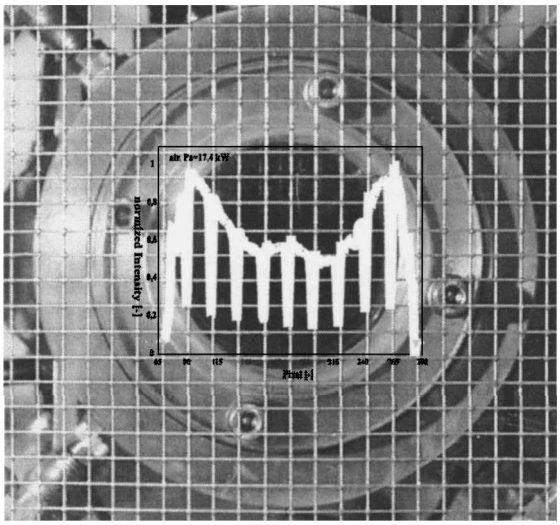

Fig. 8 Arbitrary intensity history along the x direction of the optical window of IPG3.

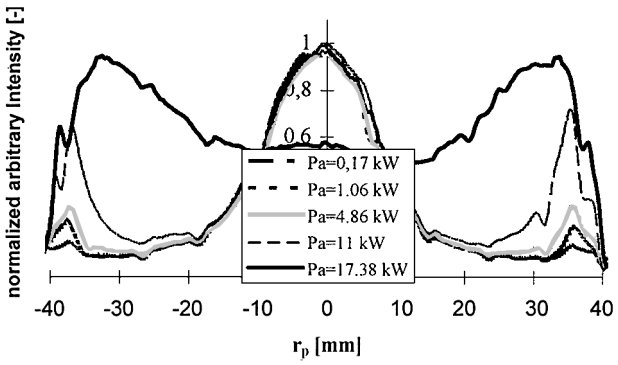

Fig. 9 Normalized relative intensities; switch from low-power mode to high-power mode (air).

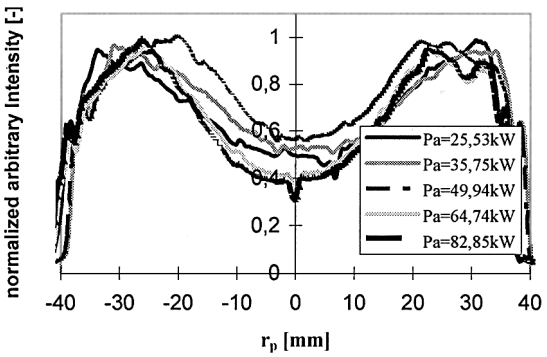

Fig. 10 Normalized relative intensities after switch from low-power mode to high-power mode.

on the increase of power must partly be used against the magnetic blocking. Figure 9 depicts the arbitrary intensity distribution for air, showing the switch from low-power mode to high-power mode.

The glow-type discharge maximum in the middle of the tube does not change in regard to its history, whereas the intensity peaks at the inner tube wall increase with increasing input power. The radial position of these peaks indicate the magnitude of an effective skin depth. In Fig. 10, the location of these maximums is at about 14–16 mm, which results in an effective skin depth of about 7–8 mm. According to Refs. 9 and 15–17, the skin depth is defined as

$$\delta = \sqrt{2/\mu_0 \sigma \omega}$$

where σ is the electrical conductivity of the plasma and ω the angular frequency of the IPG3 facility. This skin depth indicates the damping of the electric field with increasing radial distance from the induction coil. Here two major effects have to be taken into account concerning the skin depth: The cooled inner tube wall results in a (measured) decrease of the intensity. However, it is known from approximative models[16] that the dissipation rate of the power has a maximum at about 2δ. It is evident that the simple model together with the maximum of the measured relative intensities (Fig. 10) can only deliver a measure of the magnitude of the skin depth. With the transition of the discharge the intensities at the tube walls increased strongly; in the middle of the tube a weak relative maximum appeared.

Figure 10 shows the behavior of the arbitrary relative intensity curves after the discharge transition with increasing power for air operation. Generally, the intensity of the discharge increased with the power. On the other hand, the ratio between the inner wall maximum and the inner tube tends to increase. The weak maximum in the middle of the tube (see Fig. 8; $P_A = 17.38$ kW) disappeared with increasing power.

Power Characteristics of IPG3

With the plasma off (without plasma load) and the experimental conditions kept constant, the neutral gear power input could be measured. The variation of the cooling water flow has no essential influence on the neutral gear power input, shown in Figs. 11 and 12, with dependence on the anode voltage U_A.

The anode power distribution can be written, for practical considerations, in the following form:

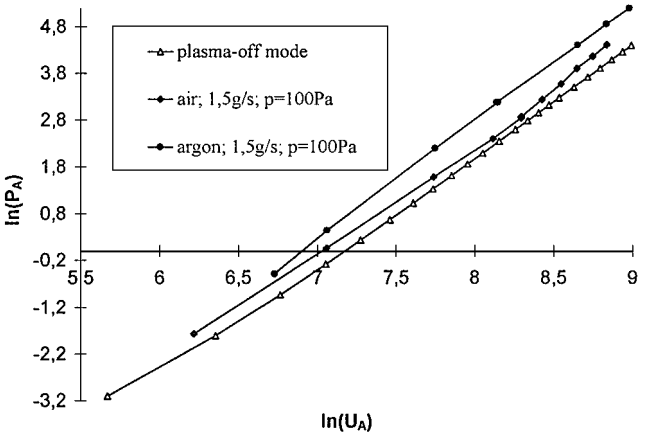

Fig. 11 Anode powers in logarithmic scale.

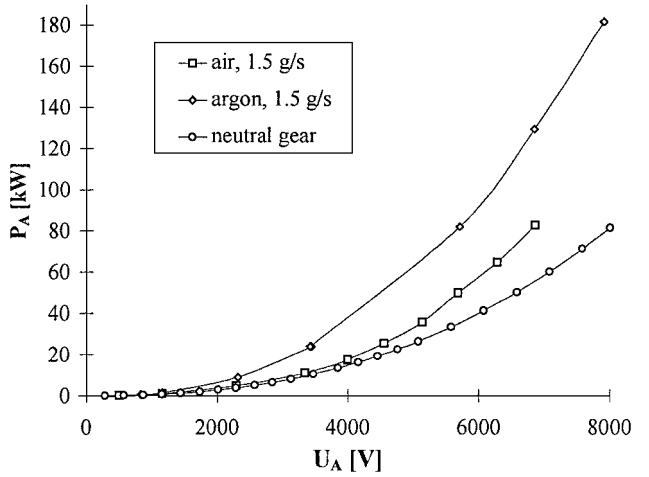

Fig. 12 Anode power vs anode voltage for argon, air, and plasma-off mode.

$$P_A = f(U_A) + aU_A^2 \approx bU_A^c$$

Here P_A is the measured anode power, U_A is the measured anode voltage, the term aU_A^2 represents the real powers, and $f(U_A)$ represents the remaining power losses such as the anode losses of the metal–ceramic triode. This leads to $P_A = bU_A^c$, with $c > 2$. This consideration is confirmed by the measured power lines (Figs. 11 and 12) that are, in a first approximation, represented by polynomial functions depending on U_A^c. Hence, the anode powers shown in a double logarithmic scale appear approximately as straight lines. Both curves were measured at an ambient/chamber pressure of about 100 Pa, a gas mass flow of 1.5 g/s, and an injection angle of 0 rad (tangential injection).

The difference between the neutral gear power and the power measured with the plasma on provides an estimation of the power that is coupled into the plasma:

$$P_{\text{Plasma}}(U_A) \approx P_{A,\text{operate}}(U_A) - P_{A,ng}(U_A)$$

Using this, a neutral-gear-power-related efficiency

$$\eta_{ng} = 1 - \frac{P_{A,ng}}{P_{A,\text{operate}}}$$

with the anode voltage U_A kept constant can be defined.[6]

Figure 13 shows the behavior of the anode current dependent on the controlled anode voltage for all three cases. Again, it can be seen that the increase of current is much higher for argon than for air.

For the ratio of the anode powers in Fig. 14, which shows the differences between the operational anode powers of argon and air more precisely, more accurately fit functions were used. This behavior could probably be explained by the properties of the plasma used. Further investigations have to be performed to describe the influences of the plasma properties such as the electrical conductivity. For example, the different absolute values and slopes of the

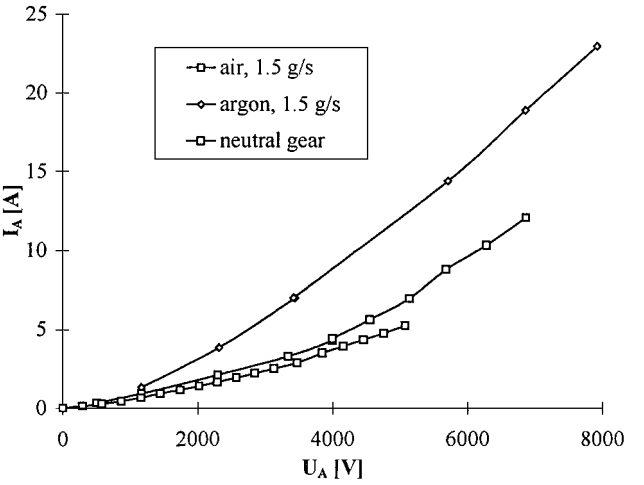

Fig. 13 Anode current vs anode voltage for argon, air, and plasma-off mode.

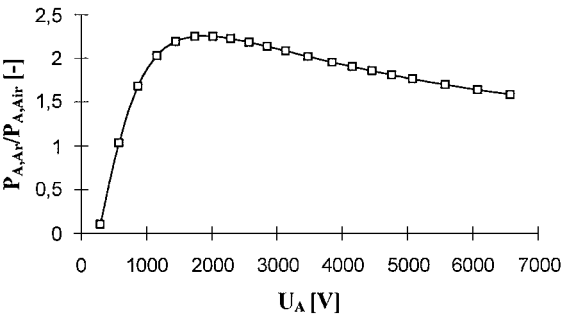

Fig. 14 $P_{A,\text{Ar}}/P_{A,\text{Air}}$ vs controlled anode voltage.

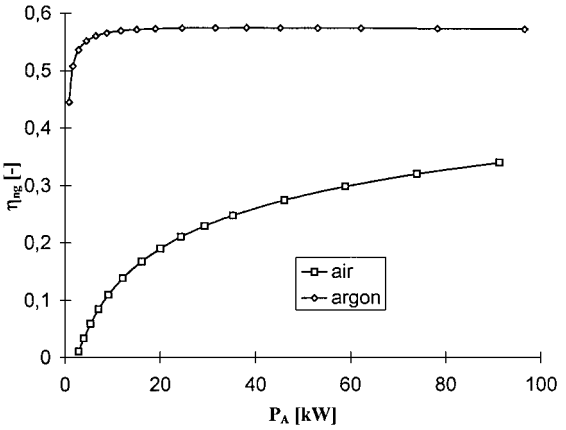

Fig. 15 Neutral-gear-related efficiency for argon and air.

electrical conductivities vs the electron temperature could explain the history of the power ratio and its maximum at $U_A \approx 1800$ V.

As the tube cooling is neglected for the neutral gear efficiency, η_{ng} represents only a raw estimation of the total efficiency. Figure 15 shows the neutral gear related efficiency depending on the anode power measured in plasma operation for the two cases.

The value for argon above $P_A \approx 100$ kW is almost constant 0.57.

Conclusions

An inductively heated plasma generator (IPG3) was developed for basic TPS material investigations using the refurbished experimental facility PWK3. Its design allows extensive investigations of the operational behavior and the characteristics of the plasma generated in the plasma tube. The different discharge behaviors for argon and air could be observed; the results enabled a rough determination of an effective skin depth for the air operation. Frequency measurements were made that showed slight differences in the field absorption behavior of argon and air. Here, further investigations for different gases in combination with planned coil current measurements will be performed to simplify the comparison with numerical results.

Concerning the power characteristics, a first comparison between argon and air operation could be made on the basis of the measurement of the Meissner-type switching anode powers. Because of the realization of the high powers, IPG3 seems to enable the aforementioned basic material tests as well as Mars or Venus reentry simulations. Therefore, future investigations will focus on the determination of heat fluxes and pressures to prepare the application of high-enthalpy reentry conditions.

Acknowledgments

The authors wish to thank the other members of the plasma wind tunnel group who helped perform the experimental investigations and who helped with their advice. Special thanks to Torsten Laux, Technical Staff Member Edgar Schreiber, Jörg Heiermann, Christian Sleziona, and Thomas Wegmann. Thanks go to research student Pia Endlich.

References

[1] Auweter-Kurtz, M., Kurtz, H., and Laure, S., "Plasma Generators for Reentry Simulation," *Journal of Propulsion and Power*, Vol. 12, No. 6, 1996, pp. 1053–1061.

[2] Bykowa, N. G., Vasil'evskii, S. A., Gordeev, A. N., Kolesnikov, A. F., Pershin, I. S., and Yakushin, M. I., "Determination of the Effective Probabilities of Catalytic Reactions on the Surfaces of Heat Shield Materials in Dissociated Carbon Dioxide Flows," *Journal of Fluid Dynamics*, Vol. 32, No. 6, 1997, pp. 876–886.

[3] Kolesnikov, A. F., and Vasil'evskii, S. A., "Results and Problems of Inductively Coupled Plasma Flows Modeling," Inst. for Problems in Mechanics, Preprint 610, Russian Academy of Science, Moscow, 1998.

[4] Bottin, B., Carbonaro, M., Zemsch, S., and Degrez, G., "Aerothermodynamic Design of an Inductively Coupled Plasma Wind Tunnel," AIAA Paper 97-2498, June 1997.

[5] Auweter-Kurtz, M., Habiger, H., and Wegmann, T., "Diagnostics of High-Enthalpy Plasma Flows," AIAA Paper 97-2495, June 1997.

[6] Wantuck, P., and Watanabe, H., "Radio Frequency (RF) Heated Supersonic Flow Laboratory," AIAA Paper 90-2469, July 1990.

[7] Vilbig, F., *Lehrbuch der Hochfrequenztechnik*, 5th ed., Vol. 2, Akademische Verlagsges, Frankfurt, Germany, 1958, Sec. 1.

[8] Technical Specification of the rf-Capacitors and the Triode RS 3300 CJ of the PWK3-IPG Energy Supply, Fritz Düsseldorf Gesellschaft, Freiburg, Germany, 1997.

[9] Mostaghimi, J., and Boulos, M. I., "Two-Dimensional Electromagnetic Field Effects in Induction Plasma Modelling," *Plasma Chemistry and Plasma Processing*, Vol. 9, No. 1, 1989, pp. 25–44.

[10] Habiger, H., and Auweter-Kurtz, M., "Investigation of High-Enthalpy Air Plasma Flow with Electrostatic Probes," *Journal of Thermophysics and Heat Transfer*, Vol. 12, No. 2, 1998, pp. 198–205.

[11] van Ootegem, B., Leborgne, L., and Vervisch, P., "Experimental Study of a Supersonic Turbulent Low Pressure Argon Plasma Jet," *Proceedings of the Third European Symposium on Aerothermodynamics for Space Vehicles*, ESA, Noordwijk, The Netherlands, 1998, pp. 105–110.

[12] Loesener, O., Auweter-Kurtz, M., Hartling, M., and Messerschmid, E., "Linear Pyrometer for Investigations of Thermal Protection Systems," *Journal of Thermophysics and Heat Transfer*, Vol. 7, No. 1, 1993, pp. 82–87; also AIAA Paper 91-1387, March 1993.

[13] Stöckle, T., Auweter-Kurtz, M., and Laure, S., "Material Catalysis in High-Enthalpy Air Flows," AIAA Paper 96-1904, June 1996.

[14] Stöckle, T., Fasoulas, S., and Auweter-Kurtz, M., "Heterogeneous Catalytic Recombination Reactions Including Energy Accommodation Considerations in High-Enthalpy Gas Flows," AIAA Paper 97-2591, June 1997.

[15] Freeman, M. P., and Chase, J. D., "Energy-Transfer Mechanism and Typical Operating Charateristics for the Thermal rf Plasma Generator," *Journal of Applied Physics*, Vol. 39, No. 1, 1968, p. 180.

[16] Eckert, H. U., "Analysis of Thermal Induction Plasmas Dominated by Radial Conduction Losses," *Journal of Applied Physics*, Vol. 41, No. 4, 1970, p. 1520.

[17] Mekideche, M. R., "Contribution à la modélisation numérique de torches de plasma d'induction," Thèse de Doctorat, Laboratoire de Recherche Techniques Inductives, École Doctorale Sciences pour l'Ingénieur de Nantes, Nantes, France, Oct. 1993.